POLITECNICO
MILANO 1863

DIPARTIMENTO DI MECCANICA

mecc

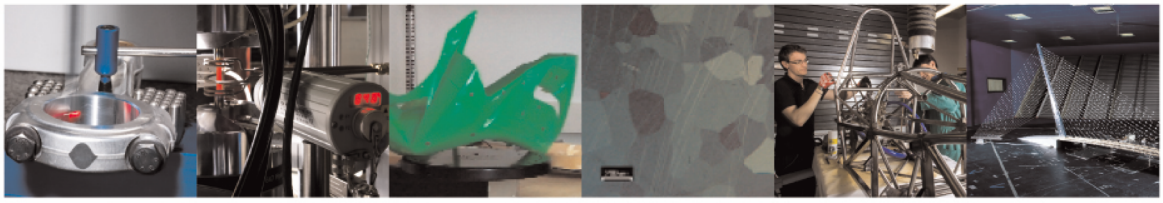

Application of the extended FASTSIM for non-Hertzian contacts towards the prediction of wear and rolling contact fatigue of wheel/rail systems

Binbin Liu, Stefano Bruni

This is a post-peer-review, pre-copyedit version of *Application of the extended FASTSIM for non-Hertzian contacts towards the prediction of wear and rolling contact fatigue of wheel/rail systems*, Binbin Liu and Stefano Bruni, Proceedings of the Institution of Mechanical Engineers, Part F: Journal of Rail and Rapid Transit 2024 238:4, 427-436. The final authenticated version is available online at: http://dx.doi.org/ 10.1177/09544097231178857

Application of the extended FASTSIM for non-Hertzian contacts towards the prediction of wear and rolling contact fatigue of wheel/rail systems

Binbin Liu *, Stefano Bruni

Dipartimento di Meccanica, Politecnico di Milano, Milan, Italy.
* E-mail: binbin.liu@polimi.it

Abstract: In this paper, the extension of the FASTSIM algorithm to a SDEC region is implemented and a strategy is proposed to generalize this algorithm to any general non-elliptic contact patch. The extended FASTSIM is applied to the prediction of wheel wear and rolling contact fatigue under typical non-Hertzian wheel/rail contact conditions, using CONTACT as a reference and showing that the extended version of FASTSIM proposed in this work provides more accurate solutions for non-Hertzian contact conditions, compared to other widely used formulations of FASTISM.

Keywords: non-Hertzian contact; non-elliptic contact; wheel/rail contact; railway wheel wear; rolling contact fatigue.

Nomenclature

a	Length of semi-axes of SDEC in longitudinal direction
b	Width of semi-axes of SDEC in lateral direction
ψ	Shape number of SDEC
y_0	Lateral shift of the origin of SDEC
N	Normal force
p_0	Maximum pressure
F_x, F_y	Longitudinal / lateral creep force
c	Equivalent radius
C_{11}, C_{13}, C_{22}, C_{23}	Linear theory coefficients for the elliptic patch
g	Ellipticity
G	Shear modulus
v_x, v_y	Longitudinal / lateral creepage
ϕ	Spin creepage
C_{11}^s, C_{13}^s, C_{22}^s, C_{23}^s	Linear theory coefficients for the SDEC patch
B_{11}, B_{22}, B_{23}	Coefficients of the second-order term as functions of the shape number
K_{13}	Coefficient of the linear term as a function of the shape number
p_x, p_y	Longitudinal / lateral stress
L_{11}, L_{13}, L_{22}, L_{23}	Flexibility parameters
x_l	Leading edge of the contact patch
τ_{max}	Traction bound
μ	Friction coefficient
L_n	Length of the non-elliptic contact patch
W_n	Width of the non-elliptic contact patch
A_n	Actual contact area
P_f	Frictional power density
V	Running velocity of the wheel
s_x, s_y	Longitudinal / lateral slip
FI	Fatigue index
μ_a	Adhesion coefficient
k	Material yield limit in shear
p_n	Normal pressure
υ	Poisson's ratio

Introduction

The modelling of the contact forces and stresses acting between a railway wheel and the rail is crucial not only for multibody system (MBS) simulation of a rail vehicle but also for the analysis of surface and sub-surface damage phenomena taking place in wheel/rail systems , particularly wear and rolling contact fatigue (RCF) [1].

The Hertz theory is widely used in wheel/rail contact modelling due to its high efficiency. However, the Hertzian assumptions are often violated for the wheel/rail contact under operational conditions since the contact patches produced by the actual wheel/rail system are often non-elliptic which restricts the application of the Hertz theory. The recent development of the wheel/rail contact modelling mainly focuses on the extension to non-Hertzian conditions for the normal contact, such as the Kik-Piotrowski (K-P) model [2], its extended version EKP [3], ANALYN [4], and semi-Hertzian [5].

In contrast, the determination of tangential forces at the wheel/rail interface in MBS simulations mostly relies on the use of the FASTSIM algorithm [6] or on specific adaptations of this method to non-Hertzian contact conditions. FASTSIM is also widely used for the wheel wear simulation and RCF estimation [7][8][9]. However, its accuracy for this purpose is not fully satisfactory [10][11] due to the issues posed by the adaptation of the method to non-Hertzian contact conditions. One way to address these issues is to approximate the contact patch as an equivalent ellipse [12], but in this case the effect of spin creepage to the longitudinal creep force is missing due to the symmetric shape of the equivalent ellipse. Alternatively, the equivalent ellipse can be used just to define the flexibility parameters of the method, whilst the calculation of the tangential stresses and local slip is performed considering the actual non-elliptic shape of the contact patch [2].

An efficient and accurate method to consider non-Hertzian contact patches is the “Kalker book of tables for non-Hertzian contacts” (KBTNH) algorithm [13][14], based on the regularization of the contact region to a Simple Double-Elliptic Contact (SDEC). This approach, however, is makes use of lookup tables which only provide the total creep forces, hence not allowing to determine the distribution of local stresses and frictional power in the contact region which are generally required for wear and RCF estimations [15].

To overcome this problem, in this paper, we apply an extended version of the FASTSIM algorithm for a SDEC region which we recently proposed [16], extending its use to a generic non-elliptic contact area and we assess the accuracy of this algorithm in the prediction of wheel wear and RCF using CONTACT as a term of comparison. The numerical results show that the extended FASTSIM provides better agreement to the results of CONTACT than other commonly used existing models for detailed analysis of wheel wear and RCF.

The paper is structured as follows. The next section summarises the approach presented in reference [16] and proposes a different strategy for the regularisation of a non-Hertzian contact patch to a SDEC region, which is more appropriate for the evaluation of wear and RCF. Then we describe the methods used for the assessment of the models considered in this study for the prediction of wear and RCF. It follows by the results for a contact region having exactly a SDEC shape and results for an actual non-Hertzian contact region obtained considering standardised wheel/rail profiles, respectively. Finally, we conclude the main observations from this study.

The extension of FASTSIM to a SDEC region

The FASTSIM algorithm was developed based on the simplified theory of rolling contact [6] and is widely used not only for the evaluation of wheel/rail creep forces but also for the

prediction of the wheel/rail surface wear and RCF in different variants [10][17][18], however, mainly restricted to elliptic contact areas. To relax this constraint, the FASTSIM algorithm has been extended to a particular group of non-elliptic shapes i.e. SDEC regions in [16].

Geometry of the SDEC region

The shape of a generic SDEC region is shown in Fig. 1 where 2*a* and 2*b* stand for the length of the contact patch in the rolling direction and the width, respectively. The origin *O* of the contact patch is located at the initial point of contact of the contacting bodies, which is shifted by y_0 from the mid-point of the patch in lateral direction.

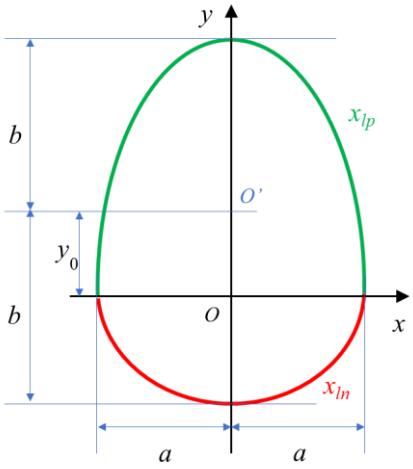

Figure 1 *Schematic of a generic SDEC patch*

The SDEC region can be expressed mathematically as follows:

$$\begin{cases} \frac{x^2}{a^2} + \frac{y^2}{b^2(1+\psi)^2} = 1 & (y > 0) \\ \frac{x^2}{a^2} + \frac{y^2}{b^2(1-\psi)^2} = 1 & (y \leq 0) \end{cases} \tag{1}$$

where the shape number, defined as:

$$\psi = y_0/b \tag{2}$$

is an indicator of the level of deviation of the contact patch shape from an ellipse and takes values ranging from -1 to 1. Clearly, the elliptic contact patch is just a particular case of SDEC when $\psi = 0$.

It should be noted that if a semi-ellipsoid normal pressure distribution is assumed in the rolling direction of a SDEC patch, the function between the normal force *N* and the maximum pressure p_0 is like for a Hertzian contact [13]:

$$N = \frac{2}{3} p_0 \pi a b \tag{3}$$

The extension of the linear theory of rolling contact and FASTSIM algorithm to a SDEC region is described in detail in reference [16] and is summarised below, as it is directly linked to the selection of the flexibility coefficients for a SDEC geometry.

Linear theory of rolling contact to a SDEC region

Applying the linear theory to the SDEC region and recalling from [16] that the effect of the longitudinal creepage component ν_x on the lateral creep force F_y and of the lateral creepage ν_y on the longitudinal force F_x are both negligible, the tangential forces read as follows:

$$\left.\begin{aligned} F_x &= -Gc^2 C_{11}^s \nu_x - Gc^3 C_{13}^s \phi \\ F_y &= -Gc^2 C_{22}^s \nu_y - Gc^3 C_{23}^s \phi \end{aligned}\right\} \tag{4}$$

where $c = \sqrt{ab}$, G is the shear modulus, ϕ is the spin creepage and C_{11}^s, C_{13}^s, C_{22}^s, and C_{23}^s are the linear theory coefficients for the SDEC patch. Note the presence of one additional coefficient C_{13}^s with respect to Kalker's linear theory for an elliptical contact patch. The need to introduce this coefficient arises from the lack of symmetry of the contact with respect to the *x* axis [16][19].

The linear theory coefficients for the SDEC patch can be determined numerically for different values of the shape number ψ using advanced contact mechanics model such as CONTACT. In [16] a simple polynomial expression of the dependence of the coefficients on the shape number is proposed as:

$$\left.\begin{aligned} C_{11}^s &= C_{11} + B_{11}\psi^2 \\ C_{13}^s &= -K_{13}\psi \\ C_{22}^s &= C_{22} + B_{22}\psi^2 \\ C_{23}^s &= C_{23} + B_{23}\psi^2 \end{aligned}\right\} \tag{5}$$

where C_{11}, C_{22} and C_{23} are the coefficients of the linear theory for the elliptic contact patch, B_{11}, B_{22} and B_{23} are the coefficients of the second-order term as functions of the shape number and K_{13} is the coefficient of the linear term as a function of the shape number. The coefficients in Equation (5) are determined numerically in reference [16] for different ellipticity values.

FASTSIM flexibility coefficients for a SEDC region

To extend the FASTSIM algorithm to the SDEC region, four flexibility parameters are used instead of the three ones used in its original version. The unsaturated stress distribution in the *x* and *y* directions over a non-elliptic contact patch reads as follows:

$$\begin{aligned} p_x(x,y) &= \left(\frac{1}{L_{11}}\nu_x - \frac{1}{L_{13}}\phi y\right)(x - x_l) \\ p_y(x,y) &= \frac{1}{L_{22}}\nu_y(x - x_l) + \frac{1}{2L_{23}}\phi\left(x^2 - x_l^2\right) \end{aligned} \tag{6}$$

with L_{11}, L_{13}, L_{22} L_{23} being four distinct flexibility parameters and x_l is the leading edge of the contact patch.

The creep forces are obtained by integrating the above equation over a SDEC region:

$$\left.\begin{aligned} F_x &= \int_{-b+y_0}^{b+y_0}\int_{-x_l}^{x_l} p_x dxdy = -\frac{8ac^2\nu_x}{3L_{11}} + \frac{2c^4\phi\psi}{L_{13}} \\ F_y &= \int_{-b+y_0}^{b+y_0}\int_{-x_l}^{x_l} p_y dxdy = -\frac{8c^2 a\nu_y}{3L_{22}} - \frac{\pi a^2 c^2 \phi}{4L_{23}} \end{aligned}\right\} \tag{7}$$

Equating term by term Equations (4) and (7) and considering Equation (5), the flexibility parameters are fully determined as functions of the linear theory coefficients for the SDEC patch as follows:

$$\left.\begin{aligned} L_{11} &= \frac{8a}{3GC_{11}^{S}} \\ L_{13} &= \frac{2c}{GK_{13}} \\ L_{22} &= \frac{8a}{3GC_{22}^{S}} \\ L_{23} &= \frac{\pi a^2}{4GcC_{23}^{S}} \end{aligned}\right\} \tag{8}$$

The unsaturated contact stresses can be determined according to Equation (6) using the flexibility parameters from Equation (8). Then, the saturation at each cell of the discretised contact patch is checked by comparing the resultant stress to a traction bound.

Different forms of the traction bound may be used in the FASTSIM algorithm. The implications of using different traction bounds in FASTSIM have been discussed in [10][21][22]. In the current study, a parabolic traction bound is assumed as follows:

$$\tau_{max}(x,y) = \mu \frac{2N}{\pi a^3 b}\left(x_l^2(y) - x^2\right) \tag{9}$$

with μ the friction coefficient and x_l the longitudinal position of the leading edge of the SDEC patch, which can be obtained from Equation (1).

Regularisation of a general non-elliptic contact area as a SEDC region

The idea to extend FASTSIM to a general non-elliptic contact area is to regularise any actual non-elliptic area to an equivalent SDEC region. To introduce the regularisation strategy used in this work, we define L_n and W_n as the length and width of the non-elliptic contact patch, i.e. the maximum distance along the rolling direction and along the lateral direction respectively between points belonging to the contact patch.

The regularisation strategy originally proposed in [13] is based on the following criteria:

(1) the area of the equivalent SDEC area is the same as the actual contact area A_n, i.e. $\pi ab = A_n$, where a and b are the semi-axes of the SDEC region.

(2) the ratio of the semi-axes of the SDEC is equal to the length to width ratio of the actual contact region, i.e. $a/b = L_n/W_n$.

(3) the origin of the SDEC patch is defined at the initial point of the contact bodies as depicted in Figure 1.

According to the above regularisation criteria, the width of the contact region is not preserved when the actual non-elliptic region is approximated to a SDEC shape. However, the contact width is an important factor in the determination of wear distribution over the contact patch and eventually across the wheel profile, so it is desirable the SDEC regularisation preserves the width of the contact patch in the *y* direction. To this aim, we introduce a modified regularisation strategy replacing criterion (2) by the following one:

(2b) set the semi-axis b of the SDEC patch to one half the width of the actual contact patch, i.e. $2b = W_n$.

Assessment of the proposed contact model

The extended FASTSIM algorithm is assessed comparing its results to other versions of FASTSIM for non-Hertzian contact conditions from the literature and to CONTACT as a term of reference. Two types of non-elliptic contact patches are considered in the assessment: the first case considers contact patches having exactly a SDEC geometry. The second case considered is a non-elliptic contact patch produced by the contact between a railway wheel having S1002 profile and a rail having UIC 60 profile.

When considering the 'exact' SDEC geometry, we assume in CONTACT a semi-ellipsoid normal pressure distribution as implemented in CONTACT [23]. We refer hereafter to the implementation of CONTACT with prescribed SDEC shape and pressure distribution as CONTACT-SDEC.

We consider three different version of FASTSIM for the assessment in the this study:

- FASTSIM-SDEC: the extension of FASTSIM for SDEC regions described in preceding section;
- FASTSIM-EQ.L: the version introduced in [2] that considers the actual non-elliptic contact region in the computation of the contact stresses and total forces, while the flexibility parameters are calculated from an equivalent ellipse;
- FASTSIM-EQ.E: the original FASTSIM algorithm for elliptic contacts is applied to an equivalent ellipse of the actual contact patch. This is essentially a Hertzian model. The equivalent ellipse is defined using the same criteria (1) and (2b) used for the regularisation of the contact patch to a SDEC shape. To ensure that the elliptic shape overlaps as much as possible with the actual non-Hertzian contact patch and given the inherent symmetry of the elliptic shape along the *y* direction, the centre of the ellipse is set at mid distance between the edges of the non-Hertzian patch in the *y* direction. It should be noted that according to the above-described approximation, the centre of the equivalent ellipse is shifted in lateral direction with respect to the initial contact point. To consider this shifting, a correction of the longitudinal creepage must be applied in the FASTSIM-EQ.E method, see [16] for more details.

Terms of assessment of the contact models

The accuracy of the different FASTSIM versions considered is assessed in regard of the prediction of wear and RCF. As far as wheel wear is concerned, the frictional power is commonly used as an indicator for wear at the wheel/rail interface, as experimental observations show that this quantity is highly correlated to abrasive wear of the contacting surfaces [24]. The frictional power is however a "global" parameter, referred to the entire contact region. For this reason, the frictional power density P_f, i.e. the frictional power per unit surface in the contact region is selected here for the assessment of wear. This quantity is defined as the scalar product of the sliding velocity times the tangential stress vectors, as given by Equation (10) for a discretized contact patch [25][26].

$$P_f(x,y) = -V \cdot \left(s_x(x,y) \cdot p_x(x,y) + s_y(x,y) \cdot p_y(x,y)\right) \quad (10)$$

where s_x and s_y are the slip components in lateral and longitudinal directions evaluated at the centre (x, y) of each cell of the discretized contact patch, and V is the running velocity of the wheel.

To compare different contact models in respect to the severity of surface initiated RCF, the outputs from the considered contact models are plotted in a shakedown map diagram, indicating the likelihood of the occurrence of surface fatigue [27]. It should be noted that the shakedown map diagram was originally derived considering full-slip of the contacting surfaces and the formation of a Hertzian contact region [27][28], whilst both these assumptions are not fulfilled in the comparisons reported below. However, the aim of this paper is not to perform a detailed analysis of surface initiated RCF for given wheel/rail contact conditions, but rather to analyse the influence of different contact models on the assessment of RCF. Hence, the full slip and Hertzian contact assumptions can be relaxed, as done also in similar investigations that can be traced in the literature [17].

To further quantify the fatigue impact with respect to surface-initiated cracks, the surface Fatigue Index (FI) proposed by Ekberg et al. [28] is computed for the selected case study, based

on different contact models. The FI is defined as a measure for the probability of RCF initiation as follows:

$$FI = \mu_a - \frac{k}{p_0} = \frac{\sqrt{F_x^2 + F_y^2}}{N} - \frac{k}{p_0} \tag{11}$$

where F_x and F_y are the longitudinal and lateral creep forces, p_0 is the maximum contact pressure, μ_a is the adhesion coefficient, and k is the material yield limit in shear, which is assumed to be 250 MPa for all cases in this paper. Damage is assumed to occur when positive values of the FI are found.

Previous studies [9][29] suggest that the accuracy of the damage analysis could be enhanced by evaluating the FI locally within a contact patch. Therefore, the local FI is computed in each cell of the discretised contact patch according to Equation (12) to obtain a better insight in the distribution of the FI over the contact patch.

$$FI(x,y) = \frac{1}{p_n(x,y)}\left(\sqrt{p_x^2(x,y) + p_y^2(x,y)} - k\right) \tag{12}$$

where $p_n(x, y)$ is the normal pressure at the cell centre (x, y).

Contact model assessment for SDEC regions

In this section, contact patches having exactly a SDEC geometry are considered. The performance of the extended FASTSIM algorithm model is evaluated under two respects by comparison to other models: the estimation of wheel wear and the prediction of RCF. To this end, we select one single value of the shape number ψ = 0.4 of a SDEC patch with the semi-axis a = 4.25 mm, ellipticity g = 1.5 for two cases: Case 1 is a pure spin condition creepage ϕ = 1.0 m^{-1} and Case 2 is a combined creepages condition from a realistic running condition suggested in reference [30] with ν_x = -0.49e-3, ν_y = -0.22e-3 and ϕ = 0.29 m^{-1}. Since the frictional power P_f defined according to Equation (10) is directly proportional to the running speed V of the wheel, a unit value V = 1.0 m/s is chosen for this parameter, to obtain a normalised value of the frictional power. The actual frictional power for a different running speed can then be obtained as the product of the normalised frictional power times the actual speed of the wheel. The material of the wheel and rail is assumed to be the same with shear modulus G = 80 GPa, Poisson's ratio υ = 0.25, and friction coefficient μ = 0.35.

Estimation of wear

To assess the performance of the contact models for the estimation of wear, the obtained frictional power density is compared to the reference result obtained using CONTACT-SDEC under three respects. First, we check if the surface distribution of the frictional power over the contact patch computed using different methods is coherent, which is relevant because this quantity is very important for detailed analysis of wear. Then, the linear distribution of the frictional power along the lateral direction in the contact patch is compared: this is a key parameter for the quantification of material removal due to abrasive wear in the simulation of wheel/rail profile evolution due to wear cumulation during service. Finally, the total power over the entire contact area is compared: this is a direct input to some global wear prediction models [31].

The surface distributions of the normalized frictional power computed for both cases are presented in Figure 2. The same conclusion can be drawn for both Case 1 i.e. the pure spin condition and Case 2 i.e. the mixed creepages condition. The results from FASTSIM-SDEC and FASTSIM-EQ.L are quite close to each other and both of them slightly overestimate the

frictional power compared to the reference result from CONTACT-SDEC. The surface distribution of the frictional power predicted by the FASTSIM-EQ.E method is qualitatively similar to the one obtained using the other methods due to the fact that the SDEC shape is not too far from an ellipse ($\psi = 0.4$). However, the maximum values of the frictional power obtained using this approximation are significantly larger than for the other two versions of FASTSIM, leading to a larger deviation from the reference solution CONTACT-SDEC, as shown in Figure 3.

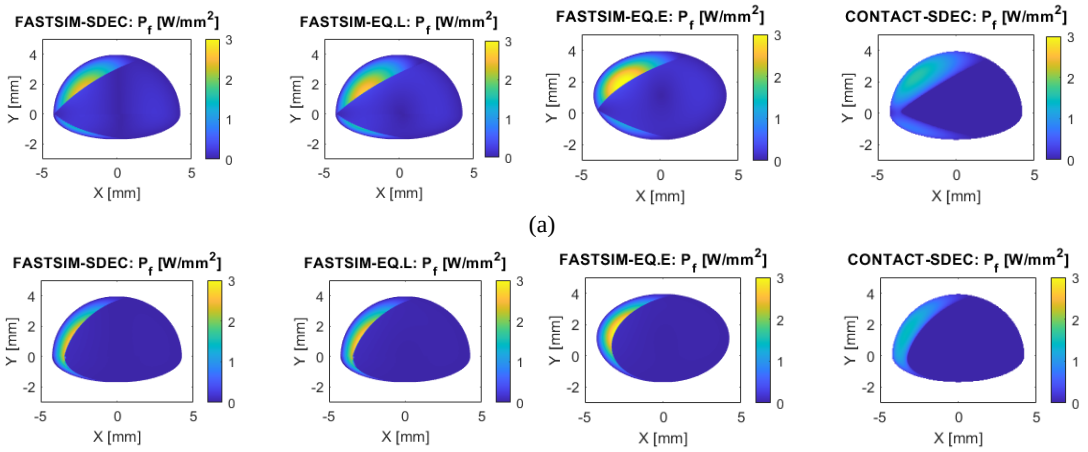

(a)

(b)

Figure 2 *Frictional power over the contact patch obtained by using different contact models for a SDEC patch (a) for Case 1 (b) for Case 2*

The depth of worn material expected at a given location across the wheel profile is directly related to the distribution of the frictional power across the contact patch in the lateral direction, which is computed by integrating the frictional power distribution along the rolling direction. The results obtained for both cases are shown in Figure 3 for the different versions of FASTSIM and for the reference solution from CONTACT-SDEC. These results show that FASTSIM-SDEC is able to well predict the wear distribution across the contact patch for the cases considered and the result from this method shows better agreement to the one from CONTACT-SDEC than both FASTSIM-EQ.L and FASTSIM-EQ.E.

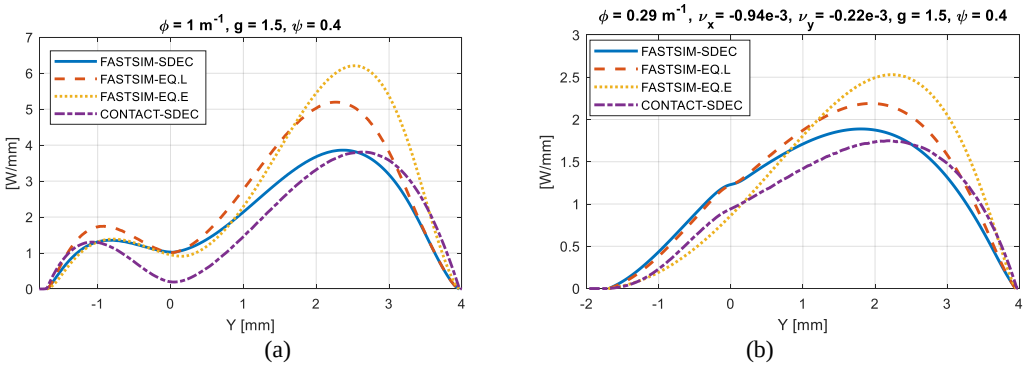

(a) (b)

Figure 3 *Frictional power across the contact patch obtained by using different contact models for a SDEC patch (a) for Case 1 (b) for Case 2*

In some simplified wear models, the total frictional power on the contact patch is selected as an indicator of severity of wear such as the wear number [31] which can be obtained by taking the ratio between the total frictional power and rolling velocity. The total power dissipated in the contact patch is computed using the results from different contact models. The values and percentage deviations with respect to CONTACT-SDEC are summarised in Table 1.

The results suggest that all simplified models overestimate the total frictional power; again

FASTSIM-SDEC shows the best agreement to the reference among all FASTSIM versions considered, with a deviation from the reference solution of 11% approximately for both cases, whereas the errors introduced by FASTSIM-EQ.L and FASTSIM-EQ.E are close to 40% and 50%, respectively, for Case 1 and the deviations are nearly halved for mixed creepages condition i.e. Case 2.

Table 1 Comparisons of the total frictional power for a SDEC patch.

Case no.	Contact model	Total power [W]	Deviation w.r.t. reference [%]
Case 1	FASTSIM-SDEC	11.5	11.4
	FASTSIM-EQ.L	14.4	40.2
	FASTSIM-EQ.E	15.4	49.8
	CONTACT-SDEC	10.3	-
Case 2	FASTSIM-SDEC	6.65	11.0
	FASTSIM-EQ.L	7.34	22.5
	FASTSIM-EQ.E	7.55	26.0
	CONTACT-SDEC	5.99	-

Prediction of RCF

The outputs for the two cases considered in this section from different contact models are plotted in a shakedown diagram as shown in Figure 4.

Although the results obtained using different contact models are in general close to each other in the shakedown map, the one predicted by FASTSIM-EQ.E deviates from CONTACT a bit more for both cases and it is already in the critical situation to cause surface fatigue for Case 1. Note the load factor is the same for all four cases because the maximum pressure is the same for all the contact models.

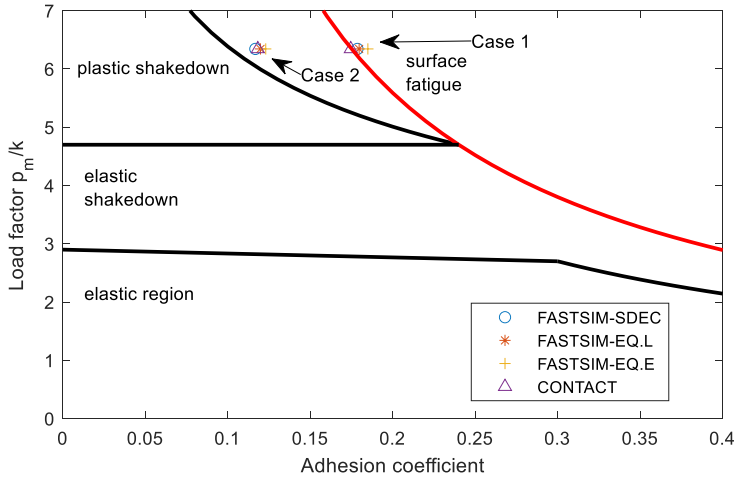

Figure 4 *Shakedown map for a SDEC patch*

The fatigue index FI is computed according to Equation (12) using results from different contact models and presented in Figure 5.

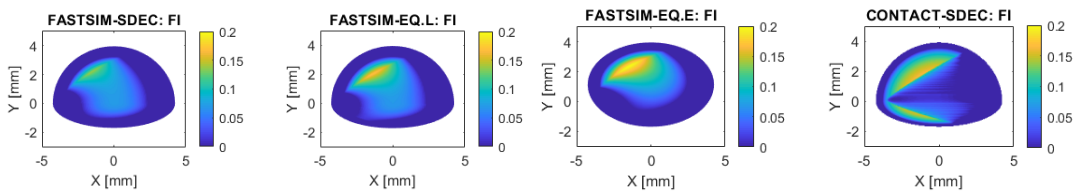

(a)

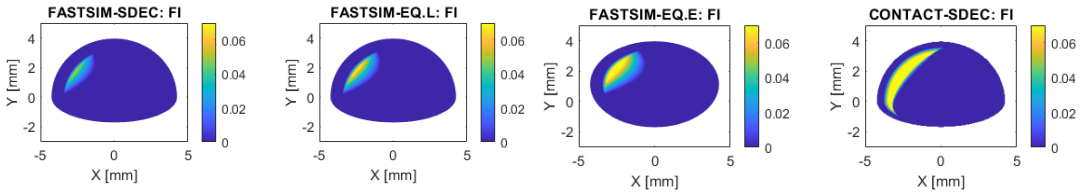

(b)

Figure 5 *FI distribution obtained by using different contact models for a SDEC patch (a) for Case 1 (b) for Case 2*

It is observed that FASTSIM-SDEC and FASTSIM-EQ.L provide better agreement to CONTACT than FASTSIM-EQ.E in terms of the distribution of the FI over the contact patch. The values predicted by FASTSIM-EQ.E are larger than those obtained from CONTACT over most part of the contact region, suggesting that FASTSIM-EQ.E overestimates the probability of RCF initiation for the considered contact condition for Case 1. For Case 2, the simplified models could not get the proper distribution of the FI and FASTSIM-SDEC and FASTSIM-EQ.L underestimate the probability of RCF initiation.

Contact model assessment for a general non-elliptic contact shape

Although the SDEC shape covers a large range of actual contact patches produced in the real wheel/rail system, some actual contact patches have non-elliptic shapes that deviate significantly from the SDEC geometry. As a typical example of this situation, we consider the contact patch produced by a wheelset with standard profile S1002 and wheel radius 460 mm in contact with a track having metric gauge (1435 mm) and UIC60 rail with 1:40 inclination. The wheelset is considered at the centered position, i.e. having zero lateral shift to the track centreline. The wheel load considered is 80 kN and the rolling velocity V = 1.0 m/s. The material of the wheel and rail is assumed to be the same with shear modulus G = 80 GPa, Poisson's ratio υ = 0.25, and friction coefficient μ = 0.35. We consider two cases: Case 1 is a pure spin condition ϕ = -0.5 m^{-1} which is meant to emphasise on the effect of non-Hertzian contact patches and Case 2 is a combined creepages condition coming from a realistic running scenario suggested in [30] with ν_x = -0.49e-3, ν_y = -0.22e-3 and ϕ = 0.29 m^{-1}.

Unlike the case of an 'exact' SDEC shape for which the contact patch geometry and the distribution of the normal pressure can be defined according to analytical expressions, in the case considered here the normal contact problem has to be solved numerically using a non-Hertzian algorithm for the solution of the normal contact. The following four combinations of algorithms for solving the normal and tangential contact problems are then considered:

- EKP+FASTSIM-SDEC: the normal contact problem is solved using the EKP approach [3], then the actual contact patch is regularised to a SDEC region based on the modified strategy proposed in this work. The regularised SDEC patch is then used to determine the four flexibility parameters required by FASTSIM-SDEC which is finally used to solve the tangential contact problem over the actual non-elliptic contact patch;
- EKP+FASTSIM-EQ.L: the normal contact problem is solved using the EKP approach, then the actual contact patch is regularised to an equivalent ellipse based on the first criterion and the modified second criterion proposed in this paper. The equivalent ellipse is used to determine the three flexibility parameters required by FASTSIM-EQ.L which is then used to solve the tangential contact problem over the actual non-elliptic contact patch;
- HZ+FASTSIM-EQ.E: the same regularisation strategy as for the previous model is applied to determine the equivalent ellipse which then completely replaces the actual contact patch for further calculations;
- CONTACT: the standard CONTACT algorithm is used to solve both the normal and tangential contact problems and serves as the reference to assess the performance of other models.

According to the modified regularisation strategy proposed in this paper, the contact region predicted by the solution of the normal problem according to the EKP method is approximated by a SDEC patch having semi-axes a = 5.8 mm and b = 10.3 mm and shape number ψ = -0.3. The same values of the semi-axes are obtained when the same non-elliptic contact region is approximated to an equivalent ellipse for use in FASTSIM-EQ.L and FASTSIM-EQ.E. The equivalent SDEC patch and the equivalent ellipse are displayed using red lines in Figure 6.

Estimation of wear

The frictional power distribution over the contact patch is calculated using the above-mentioned four combinations of algorithms for solving the normal and tangential contact problems and the results are illustrated in Figure 6.

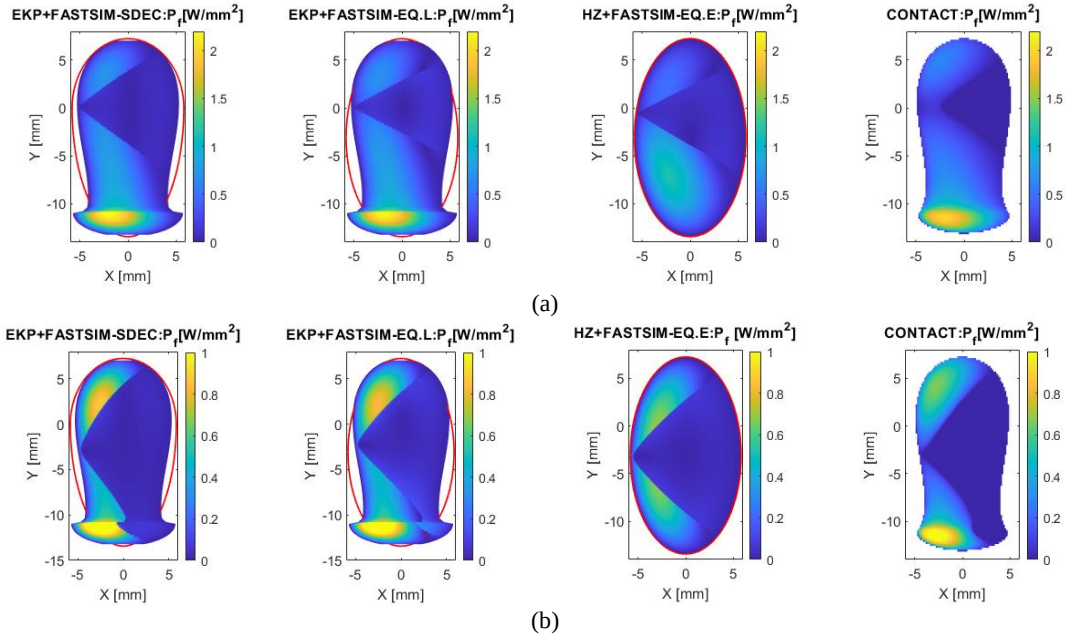

Figure 6 *Frictional power distribution obtained by using different contact models for the contact pair of S1002/UIC60 (a) for Case 1 (b) for Case 2*

The same conclusions can be achieved for both cases. It is seen that both the EKP+FASTSIM-SDEC and the EKP+FASTSIM-EQ.L can well predict the distribution of the frictional power over the contact patch, but the maximum value is slightly underestimated. The Hertzian model HZ+FASTSIM-EQ.E, instead, underestimates the frictional power in the entire contact region.

The frictional power per unit length across the contact patch for this case is plotted in Figure 7 for the four contact models. The results indicate a good agreement of EKP+FASTSIM-SDEC, EKP+FASTSIM-EQ.L and CONTACT. In addition, EKP+FASTSIM-SDEC is better than EKP+FASTSIM-EQ.L in the region from -5 mm to 5 mm of the contact patch for both cases and also in the peak region towards the flange (negative values of coordinate y) for Case 2. The Hertzian model HZ+FASTSIM-EQ.E fails to capture the actual distribution of the frictional power across the contact patch and, in particular, totally misses to reproduce the concentration of the frictional power in the portion of the contact region towards the wheel flange.

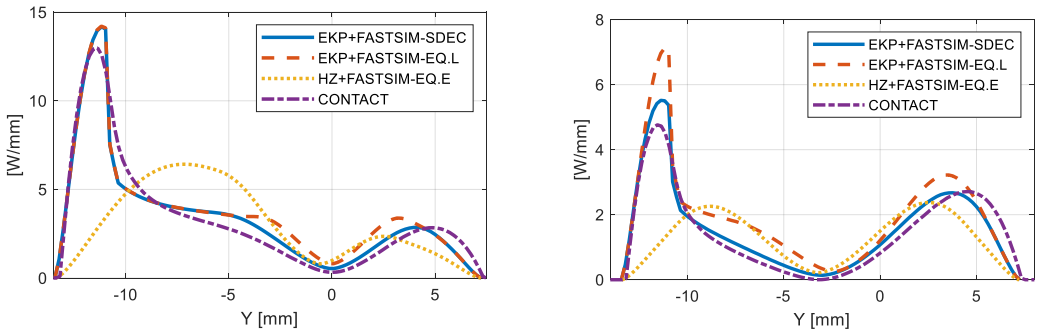

Figure 7 *Frictional power across the contact patch obtained by using different contact models for the contact pair of S1002/UIC60 (a) for Case 1 (b) for Case 2*

The total frictional power computed using the results from different contact models and the percentage deviation with respect to CONTACT are reported in Table 2. It is seen that that EKP+FASTSIM-SDEC shows the best agreement to the reference for both cases. The difference is approximately 4% and 7%, respectively for Cases 1 and 2, whereas EKP+FASTSIM-EQ.L overestimates the frictional power by 11% for Case 1 and 33% for Case 2 and HZ+FASTSIM-EQ.E underestimates this value by approximately 9% for Case 1 and 12% for Case 2 while missing completely to capture the distribution of the frictional power across the contact patch, as shown above.

Table 2 Comparisons of the total frictional power for the contact pair of S1002/UIC60.

Case no.	Contact model	Total power [W]	Deviation w.r.t. reference [%]
Case 1	EKP+FASTSIM-SDEC	71.1	3.64
	EKP+FASTSIM-EQ.L	76.5	11.5
	HZ+FASTSIM-EQ.E	62.5	-8.89
	CONTACT	68.6	-
Case 2	EKP+FASTSIM-SDEC	32.5	6.91
	EKP+FASTSIM-EQ.L	40.5	33.2
	HZ+FASTSIM-EQ.E	26.6	-12.5
	CONTACT	30.4	-

Prediction of RCF

The outputs of the current case study obtained using different contact models are indicated in the shakedown map shown in Figure 8.

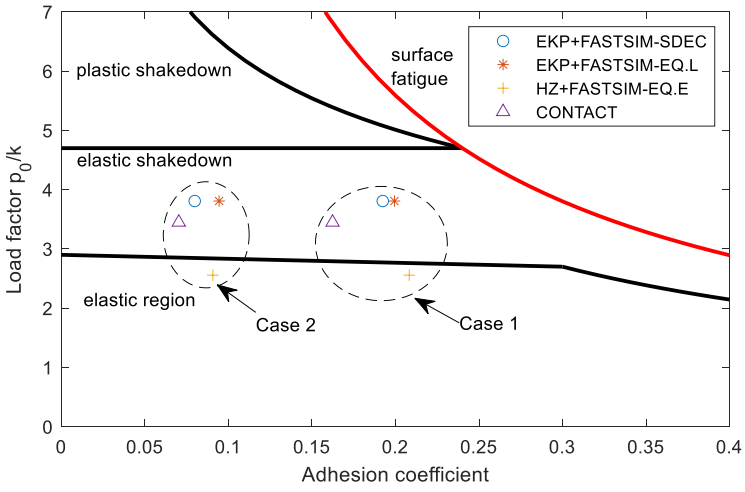

Figure 8 *Shakedown map for the contact pair of S1002/UIC60*

In this case, the results obtained from different contact models are located in different regions

of the shakedown map, resulting in different predictions regarding the chances of RCF occurring for the considered contact cases. We note the scatter of the points in the shakedown map is much greater in this case compared to the case treated in the preceding section for a SDEC patch. This is partly due to differences in the load factor arising from the use of different methods to solve the normal problem. The predictions of EKP+FASTSIM-SDEC and EKP+FASTSIM-EQ.L are very close to each other in quite good agreement with CONTACT, whereas the prediction based on the HZ+FASTSIM-EQ.E shows a quite large deviation from CONTACT.

The distribution of FI over the contact patch is computed for the two cases as shown in Figure 9. The results found for FASTSIM-SDEC combined with EKP are in very good agreement with the reference result obtained using CONTACT. In contrast, EKP+FASTSIM-EQ.L overestimates the probability of RCF initiation in the portion of the contact region close to the origin (initial contact point). The Hertzian model HZ+FASTSIM-EQ.E seems not suitable for this application because it completely fails to capture the distribution of the FI over the contact patch for both cases.

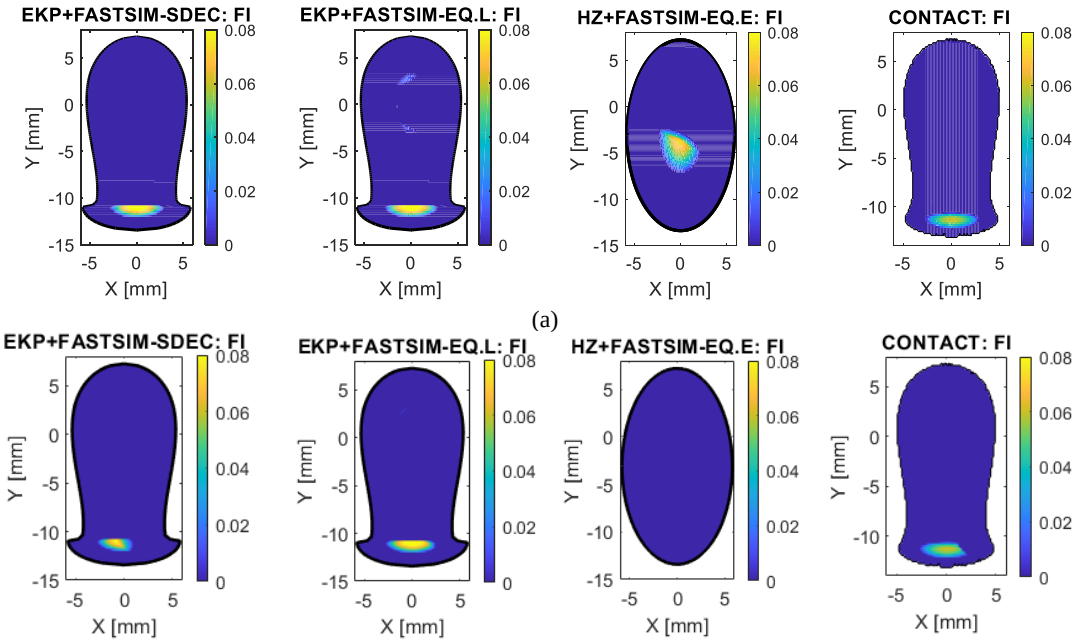

Figure 9 *FI distribution obtained by using different contact models for the contact pair of S1002/UIC60 (a) for Case 1 (b) for Case 2*

Conclusions

The extended FASTSIM algorithm has been applied for the prediction of wear under non-elliptic contact conditions for two types of contact patches, namely theoretical SDEC patches and actual highly non-Hertzian patches corresponding to a contact condition which is representative of an actual wheel/rail profile combination.

The numerical results presented in the paper show that the extended FASTSIM provides good agreement to the CONTACT algorithm in terms of wheel wear estimation and prediction of the initiation of rolling contact fatigue damage on the wheel contact surface which is a challenging task for most contact models. The comparative analyses reported in the paper show that the extended FASTSIM offers results in better agreement with the reference model CONTACT compared to the other FASTSIM versions considered in this study, without loss of computational efficiency. In particular, the proposed extension of the FASTSIM algorithm appears to be well suited to address the estimation of wear and RCF for non-Hertzian contact

conditions under relatively large values of spin creepage. Therefore, we conclude that the extended FASTSIM algorithm is a fast but accurate method for the analysis of wear and RCF damage in wheel/rail contact considering the trade-off between the computational efficiency and accuracy. One inherent limitation of the results presented in this work is that the accuracy of the different FASTSIM versions could only by assessed in terms of comparison to numerical results from CONTACT. This latter algorithm is based on a more refined representation of the local elastic deformation of the contacting bodies than FASTSIM, and there is a general consensus that it can be considered as a reference for rolling contact problems relevant to railway engineering. Yet, an examination of the performance of different FASTSIM versions based on the use of experimental data would represent a challenging but useful extension of this work.

Future work will focus on the incorporation of the extended FASTSIM in MBS simulation of rail vehicle dynamics, to further assess the performance of the algorithm for the determination of the contact forces and the damage analysis of wheel/rail contact surface in a wide range of operational scenarios.

References

[1] S. Iwnicki, Ed., *Handbook of Railway Vehicle Dynamics*. Boca Raton: Taylor & Francis, 2006.

[2] J. Piotrowski and W. Kik, "A simplified model of wheel/rail contact mechanics for non-Hertzian problems and its application in rail vehicle dynamic simulations," *Veh. Syst. Dyn.*, vol. 46, no. 1–2, pp. 27–48, 2008.

[3] B. Liu, S. Bruni, and E. Vollebregt, "A non-Hertzian method for solving wheel–rail normal contact problem taking into account the effect of yaw," *Veh. Syst. Dyn.*, vol. 54, no. 9, pp. 1226–1246, 2016.

[4] M. Sh. Sichani, R. Enblom, and M. Berg, "A novel method to model wheel–rail normal contact in vehicle dynamics simulation," *Veh. Syst. Dyn.*, vol. 52, no. 12, pp. 1752–1764, 2014.

[5] J. Ayasse and H. Chollet, "Determination of the wheel rail contact patch in semi-Hertzian conditions," *Veh. Syst. Dyn.*, vol. 43, no. 3, pp. 161–172, 2005.

[6] J. J. Kalker, "A Fast Algorithm for the Simplified Theory of Rolling Contact," *Veh. Syst. Dyn.*, vol. 11, no. 1, pp. 1–13, 1982.

[7] F. Braghin, R. Lewis, R. S. Dwyer-Joyce, and S. Bruni, "A mathematical model to predict railway wheel profile evolution due to wear," *Wear*, vol. 261, no. 11–12, pp. 1253–1264, 2006.

[8] T. Jendel, "Prediction of wheel profile wear-comparisons with field measurements," *Wear*, vol. 253, pp. 89–99, 2002.

[9] B. Dirks and R. Enblom, "Prediction model for wheel profile wear and rolling contact fatigue," *Wear*, vol. 271, no. 1–2, pp. 210–217, 2011.

[10] B. Liu, S. Bruni, and R. Lewis, "Numerical calculation of wear in rolling contact based on the Archard equation: Effect of contact parameters and consideration of uncertainties," *Wear*, vol. 490–491, no. November 2021, p. 204188, 2021.

[11] R. Enblom and M. Berg, "Impact of non-elliptic contact modelling in wheel wear simulation," *Wear*, vol. 265, no. 9–10, pp. 1532–1541, 2008.

[12] E. A. H. Vollebregt, C. Weidemann, and A. Kienberger, "Use of 'CONTACT' in Multi-Body Vehicle Dynamics and Profile Wear Simulation: Initial Results," *22nd Int. Symp. Dyn. Veh. Roads Tracks*, pp. 1–6, 2011.

[13] J. Piotrowski, B. Liu, and S. Bruni, "The Kalker book of tables for non-Hertzian contact of wheel and rail," *Veh. Syst. Dyn.*, vol. 55, no. 6, pp. 875–901, 2017.

[14] J. Piotrowski, S. Bruni, B. Liu, and E. Di Gialleonardo, "A fast method for determination of creep forces in non-Hertzian contact of wheel and rail based on a book of tables," *Multibody Syst Dyn*, vol. 45, pp. 169–184, 2019.

[15] N. Bosso, M. Magelli, and N. Zampieri, *Simulation of wheel and rail profile wear: a*

review of numerical models, vol. 30, no. 4. Springer Nature Singapore, 2022.
[16] B. Liu, B. Fu, and S. Bruni, "Generalisation of the linear theory of rolling contact to a single double-elliptic contact region and its application to solve non-Hertzian contact problems using extended FASTSIM," *Veh. Syst. Dyn.*, no. 10.1080/00423114.2022.2113808, 2022.
[17] S. Hossein-Nia, M. S. Sichani, S. Stichel, and C. Casanueva, "Wheel life prediction model–an alternative to the FASTSIM algorithm for RCF," *Veh. Syst. Dyn.*, vol. 56, no. 7, pp. 1051–1071, 2018.
[18] R. Enblom and M. Berg, "Simulation of railway wheel profile development due to wear influence of disc braking and contact environment," *Wear*, vol. 258, no. 7–8, pp. 1055–1063, 2005.
[19] E. Vollebregt, "Comments on 'the Kalker book of tables for non-Hertzian contact of wheel and rail,'" *Veh. Syst. Dyn.*, vol. 56, no. 9, pp. 1451–1459, 2018.
[20] J. J. Kalker, *Three dimensional elastic bodies in rolling contact*. Dordrecht/Boston/London: Kluwer Academic Publishers, 1990.
[21] E. A. H. Vollebregt and P. Wilders, "FASTSIM2: A second-order accurate frictional rolling contact algorithm," *Comput. Mech.*, vol. 47, no. 1, pp. 105–116, 2011.
[22] M. Sh. Sichani, R. Enblom, and M. Berg, "An alternative to FASTSIM for tangential solution of the wheel–rail contact," *Veh. Syst. Dyn.*, vol. 54, no. 6, pp. 748–764, 2016.
[23] E. A. H. Vollebregt, "Contact Mechanics Computing & Consulting," 2018.
[24] H. Krause and G. Poll, "Wear of wheel-rail surfaces," *Wear*, vol. 113, no. 1, pp. 103–122, 1986.
[25] F. Braghin, S. Bruni, and F. Resta, "Wear of railway wheel profiles: A comparison between experimental results and a mathematical model," *Veh. Syst. Dyn.*, vol. 37, no. SUPPL., pp. 478–489, 2003.
[26] I. Kaiser, G. Poll, and J. Vinolas, "Modelling the impact of structural flexibility of wheelsets and rails on the wheel-rail contact and the wear," *Wear*, no. August, p. 203445, 2021.
[27] K. L. Johnson, *Contact Mechanics*. Cambridge, UK: Cambridge University Press, 1985.
[28] A. Ekberg, E. Kabo, and H. Andersson, "An engineering model for prediction of rolling contact fatigue of railway wheels," *Fatigue Fract. Eng. Mater. Struct.*, vol. 25, no. 10, pp. 899–909, 2002.
[29] B. Dirks, R. Enblom, A. Ekberg, and M. Berg, "The development of a crack propagation model for railway wheels and rails," *Fatigue Fract. Eng. Mater. Struct.*, vol. 38, no. 12, pp. 1478–1491, 2015.
[30] E. Roger and M. Berg, "Towards calibrated wheel wear simulation-a comparison between traditional approach and novel methods," in *6th International Conference on Railway Bogies and Running Gears*, 2004, pp. 181–190.
[31] T. G. Pearce and N. D. Sherratt, "Prediction of wheel profile wear," *Wear*, vol. 144, no. 1–2, pp. 343–351, 1991.